Available online at www.sciencedirect.com
SCIENCE DIRECT®
Coastal Engineering 48 (2003) 243–256
Coastal Engineering
An International Journal for Coastal, Harbour and Offshore Engineers
www.elsevier.com/locate/coastaleng

Effects of cross-shore boundary condition errors in nearshore circulation modeling

Qin Chen[a,*], Ib A. Svendsen[b]

[a] Department of Civil Engineering, University of South Alabama, Mobile, AL 36688, USA
[b] Center for Applied Coastal Research, University of Delaware, Newark, DE 19716, USA

Received 31 May 2002; accepted 16 April 2003

Abstract

The paper analyzes the effect which prescribed errors in the cross-shore boundary conditions for a computational domain along a beach have on the flow field predicted inside the domain. This problem is relevant because errors in boundary conditions are unavoidable when modeling limited domains of a nearshore region. For simplicity, we consider a longshore uniform plane beach with monochromatic, obliquely incident waves, and assume depth uniform currents. It is then studied analytically and numerically how small perturbations of the boundary conditions along both upstream and downstream cross-shore boundaries spread inside the computational domain. It is found that the errors at the upstream cross-shore boundary tend to spread over a long distance downstream of the boundary, while the influence of the errors in the downstream boundary condition is limited to the adjacent upstream area of the computational domain. Both the numerical and analytical solutions show that the errors introduced at the upstream boundary decay exponentially in the surf zone at a rate proportional to the bottom friction. A simple formula is developed to estimate the influence distance of the upstream errors. If we consider the mismatch in the volume flux at the upstream boundary, the error merely redistributes in the cross-shore direction to conserve volume. In the case of excessive flux or velocity specified at the cross-shore boundaries, a circulation cell tends to appear in the offshore region where the errors caused by the boundary mismatch increase with the cross-shore width of the model domain.

Keywords: Longshore current; Boundary conditions; Nearshore circulation; Perturbation analysis; Numerical model; NSW equations; Dispersive mixing

1. Introduction

In nearshore modeling, it is only possible to simulate waves and currents in a small domain of the ocean. The boundary conditions along the free boundaries facing the ocean in the cross-shore and the longshore directions represent the effect of the flow outside the computational domain, which is not modeled and therefore by definition is unknown. Therefore, unless special information is known about the outside flow conditions, these boundary conditions will always be estimates only and hence subject to errors relative to actual flow patterns.

* Corresponding author. Fax: +1-251-461-1400.
E-mail address: qchen@jaguar1.usouthal.edu (Q. Chen).

0378-3839/03/$ - see front matter © 2003 Elsevier B.V. All rights reserved.
doi:10.1016/S0378-3839(03)00030-9

The question therefore arises: how important are errors in the specified boundary conditions along such free boundaries to the predictions of the flow inside the domain? Is it conceivable that under ideal conditions the computational domain could be made large enough so that the region of actual interest is far enough away from the boundaries to make the boundary errors insignificant? How large should a computational domain be to achieve such insignificant boundary errors?

The problem of boundary conditions for a limited model domain has mainly been discussed in connection with laboratory experiments of longshore currents. Dalrymple et al. (1977), Visser (1991), Reniers and Battjes (1997), and Hamilton and Ebersole (2001), among others, demonstrated that a virtually uniform longshore current could be obtained in a portion of the model basin in the laboratory by minimizing the circulation in the offshore region resulting from the errors at the upstream and downstream boundaries. Our understanding of the influence of the cross-shore boundary conditions on the longshore current simulations, however, is still very limited and consequently no tool is available to quantitatively estimate such boundary effects in the modeling of nearshore circulation.

The present paper analyzes how prescribed errors in the boundary conditions along both upstream and downstream cross-shore boundaries spread inside the computational domain. The paper is organized as follows. We first briefly describe the complete model used in the numerical simulations and as a basis for the approximations introduced to transform the model equations to a form that can be solved analytically. Next, a perturbation method is used to develop a set of equations governing the spreading of the errors introduced at the cross-shore boundaries in the computational domain. Separate approximated equations are obtained for the region downstream of the upstream boundary, and for the region upstream of the downstream boundary. An analytical solution is obtained from the perturbed equations, which describes the influence of the upstream boundary errors on the flow field inside the domain. The numerical solutions are then compared with the analytical results followed by an analysis of the momentum and mass balance of the computed flow field. Finally, the findings and conclusions are summarized.

2. Theoretical analysis

2.1. Basic equations

The basic equations describing the nearshore circulation we are considering are essentially the equations of the quasi-3D SHORECIRC model (SC) developed at the University of Delaware. They are based on the depth-integrated, time-averaged equations of continuity and momentum, which in complete form and in tensor notation read:

$$\frac{\partial \bar{\zeta}}{\partial t}+\frac{\partial \bar{Q}_\alpha}{\partial x_\alpha}=0 \tag{1}$$

$$\begin{aligned}\frac{\partial \bar{Q}_\beta}{\partial t}&+\frac{\partial}{\partial x_\alpha}\left(\frac{\bar{Q}_\alpha \bar{Q}_\beta}{h}\right)+\frac{\partial}{\partial x_\alpha}\int_{-h_0}^{\bar{\zeta}} V_{1\alpha}V_{1\beta}\mathrm{d}z\\&+\frac{\partial}{\partial x_\alpha}\overline{\int_{\zeta_t}^{\zeta} u_{w\alpha}V_{1\beta}+u_{w\beta}V_{1\alpha}\mathrm{d}z}+g(h_0+\bar{\zeta})\frac{\partial \bar{\zeta}}{\partial x_\beta}\\&-\frac{\tau_\beta^{\mathrm{S}}}{\rho}+\frac{\tau_\beta^{\mathrm{B}}}{\rho}+\frac{1}{\rho}\frac{\partial}{\partial x_\alpha}\left(S_{\alpha\beta}-\overline{\int_{-h_0}^{\zeta}\tau_{\alpha\beta}\mathrm{d}z}\right)=0\end{aligned} \tag{2}$$

Here the total volume flux $\bar{Q}_\alpha$ is defined by

$$\bar{Q}_\alpha=\int_{-h_0}^{\bar{\zeta}} u_\alpha \mathrm{d}z \tag{3}$$

where u_α is the total velocity at any point of the flow.

$S_{\alpha\beta}$ is the radiation stress, which is defined as

$$S_{\alpha\beta}\equiv\overline{\int_{-h_0}^{\zeta}(p\delta_{\alpha\beta}+\rho u_{w\alpha}u_{w\beta})\mathrm{d}z}-\delta_{\alpha\beta}\frac{1}{2}\rho g h^2 \tag{4}$$

where $u_{w\alpha}$ is the horizontal shortwave-induced velocity. $\tau_{\alpha\beta}$ represents the horizontal turbulent stresses in the fluid, while τ_β^{S} and τ_β^{B} are the surface and bottom shear stresses, respectively.

In these general equations, the total current velocity, V_α, is defined as the time average of u_α, and $V_{1\alpha}$ is then the depth varying part of V_α. The third and fourth (integral) terms in the momentum equation represent the effect of the depth variation of the current on the horizontal distribution of volume flux $\bar{Q}_\alpha$, the so-called dispersive mixing. It was found by Svendsen and Putrevu (1994) that this mechanism in e.g. long-

shore currents far overshadows the mixing effects of the breaker-generated turbulence.

In the numerical simulations described later, these equations are solved with $S_{\alpha\beta}$ and $Q_{w\alpha}$ determined from the wave model REF/DIF (Kirby and Dalrymple, 1994).

2.2. Approximate equations for the analytical solution

In order to better understand the problem considered, it is desirable also to develop an approximate analytical solution. For that purpose the general equations described above are simplified by assuming that the dispersive mixing terms and the lateral mixing from the turbulent stresses can be combined and approximated by a traditional diffusion coefficient. The value of the coefficient is determined based on the experience with the numerical solutions of the SC-equations. In addition, we write the bottom friction by a (linearised) expression based on a friction factor f.[1]

This approach reduces the general equations to the following form written in the Cartesian (x,y) components to facilitate the following development

$$\frac{\partial \zeta}{\partial t}+\frac{\partial Q_x}{\partial x}+\frac{\partial Q_y}{\partial y}=0 \tag{5}$$

$$\frac{\partial Q_x}{\partial t}+\frac{\partial}{\partial x}\left(\frac{Q_x^2}{h}\right)+\frac{\partial}{\partial y}\left(\frac{Q_xQ_y}{h}\right)+gh\frac{\partial \zeta}{\partial x} =-\frac{1}{\rho}\left(\frac{\partial S_{xx}}{\partial x}+\frac{\partial S_{yx}}{\partial y}\right)-\frac{f}{h^2}Q_x\sqrt{Q_x^2+Q_y^2}+M_x \tag{6}$$

$$\frac{\partial Q_y}{\partial t}+\frac{\partial}{\partial x}\left(\frac{Q_xQ_y}{h}\right)+\frac{\partial}{\partial y}\left(\frac{Q_y^2}{h}\right)+gh\frac{\partial \zeta}{\partial y} =-\frac{1}{\rho}\left(\frac{\partial S_{xy}}{\partial x}+\frac{\partial S_{yy}}{\partial y}\right)-\frac{f}{h^2}Q_y\sqrt{Q_x^2+Q_y^2}+M_y \tag{7}$$

where Q_x and Q_y are the cross-shore and longshore volume fluxes, ζ is the free surface elevation averaged over the short wave period, $S_{\alpha\beta}$ as before is the radiation stress owing to the short wave motion, h is the total water depth, and g is the gravitational acceleration. In addition, M_x and M_y are the lateral mixing terms replacing the dispersive mixing terms as follows

$$M_x=2\frac{\partial}{\partial x}\left[Dh\frac{\partial}{\partial x}\left(\frac{Q_x}{h}\right)\right]+\frac{\partial}{\partial y}\left[Dh\frac{\partial}{\partial y}\left(\frac{Q_x}{h}\right)\right] +\frac{\partial}{\partial y}\left[Dh\frac{\partial}{\partial x}\left(\frac{Q_y}{h}\right)\right] \tag{8}$$

$$M_y=2\frac{\partial}{\partial y}\left[Dh\frac{\partial}{\partial y}\left(\frac{Q_y}{h}\right)\right]+\frac{\partial}{\partial x}\left[Dh\frac{\partial}{\partial x}\left(\frac{Q_y}{h}\right)\right] +\frac{\partial}{\partial x}\left[Dh\frac{\partial}{\partial y}\left(\frac{Q_x}{h}\right)\right] \tag{9}$$

where D is the lateral mixing coefficient that includes the contributions from the turbulence and dispersive mixing owing to depth variations of the current. Eqs. (5)–(9) are the basis for the following theoretical analysis of the problem. These equations are essentially the NSW equations with the forcing, bottom friction and diffusion terms. They have been commonly used in the past for the modeling of breaking-generated nearshore horizontal circulation.

There are four physical boundaries that need to be specified in a nearshore circulation model. We will limit our study to the boundary conditions normal to the shoreline and leave out the effects of the offshore boundary and the moving shoreline conditions because much less attention has been paid to the influence of cross-shore boundary conditions in the literature.

2.3. Perturbation analysis

In order to gain insight into the physical mechanisms behind the spreading of errors imposed at the cross-shore boundaries, we analyze the governing equations using a perturbation expansion of the type

$$\zeta=\zeta^{(0)}+\epsilon\zeta^{(1)}+\cdots;\quad Q_x=Q_x^{(0)}+\epsilon Q_x^{(1)}+\cdots;\quad Q_y=Q_y^{(0)}+\epsilon Q_y^{(1)}+\cdots \tag{10}$$

where ϵ is the expansion parameter that is smaller than unity, and the superscript 0 denotes the assumed

[1] Note that in the formulation used here f is only half the value of the friction factor normally used in SC applications.

longshore uniformed background flow and the equivalent boundary conditions and 1 denotes the flow disturbances caused by the errors or mismatch imposed along the cross-shore boundaries. The magnitude of the boundary disturbance is assumed to be weaker than that of the background flow generated by wave breaking. For simplicity, we consider that the disturbed flow has developed to a steady state, and the beach is longshore uniform and plane. Consequently, we have $\partial/\partial t = 0$ in both the background and residual flows, and $\partial/\partial y = 0$ in the background flow only.

Substituting Eq. (10) into Eqs. (5)–(7) and collecting the terms with the same ordering lead to the zero-order equations governing the wave setup and longshore uniform current generated by wave breaking

$$\frac{\partial Q_x^{(0)}}{\partial x} = 0 \tag{11}$$

$$gh\frac{\partial \zeta^{(0)}}{\partial x} = -\frac{1}{\rho}\left(\frac{\partial S_{xx}}{\partial x}\right) \tag{12}$$

$$\frac{1}{\rho}\frac{\partial S_{xy}}{\partial x} + \frac{f}{h^2}Q_y^{(0)}\,|\,Q_y^{(0)}\,| - \frac{\partial}{\partial x}\left[Dh\frac{\partial}{\partial x}\left(\frac{Q_y^{(0)}}{h}\right)\right] = 0 \tag{13}$$

and to the first-order equations

$$\frac{\partial Q_x^{(1)}}{\partial x} + \frac{\partial Q_y^{(1)}}{\partial y} = 0 \tag{14}$$

$$\frac{Q_y^{(0)}}{h}\frac{\partial Q_x^{(1)}}{\partial y} + gh\frac{\partial \zeta^{(1)}}{\partial x} = -\frac{f}{h^2}Q_x^{(1)}\,|\,Q_y^{(0)}\,| + M_x^{(1)} \tag{15}$$

$$Q_x^{(1)}\frac{\partial}{\partial x}\left(\frac{Q_y^{(0)}}{h}\right) + \frac{Q_y^{(0)}}{h}\frac{\partial Q_y^{(1)}}{\partial y} + gh\frac{\partial \zeta^{(1)}}{\partial y} = -\frac{2f}{h^2}Q_y^{(1)}\,|\,Q_y^{(0)}\,| + M_y^{(1)} \tag{16}$$

where $M_x^{(1)}$ and $M_y^{(1)}$ are the disturbances in the lateral mixing terms owing to the cross-shore boundary errors.

It is well known that Eqs. (12) and (13) are the classic equations governing the wave setup and longshore uniform current generated by wave breaking. The first-order Eqs. (14)–(16) govern the additional flow induced by the errors in the cross-shore boundary conditions.

3. Analytical solution

To obtain an analytical solution to the first-order equations governing the spatial distribution of the errors caused by the cross-shore boundary mismatches, simplifications are needed. First, we focus on the area where the longshore current is located. If there were no boundary mismatches, a uniform longshore current would exist in this region as a balance between the cross-shore gradient of the radiation stress S_{yx}, the bottom friction, and the lateral mixing. The longshore pressure gradient is obviously absent in the zero order momentum balance. In the first-order governing equations it may be reasonable to assume that the disturbances in the longshore pressure gradient and the lateral mixing owing to errors in the cross-shore boundary conditions are small in comparison with other terms. The justification of this assumption will be given in the later section in connection with the analysis of the momentum balance based on the numerical model solutions.

Neglecting the longshore pressure gradient and diffusion terms, Eqs. (15) and (16) reduce to

$$\frac{Q_y^{(0)}}{h}\frac{\partial Q_x^{(1)}}{\partial y} + gh\frac{\partial \zeta^{(1)}}{\partial x} = -\frac{f}{h^2}Q_x^{(1)}\,|\,Q_y^{(0)}\,| \tag{17}$$

$$Q_x^{(1)}\frac{\partial}{\partial x}\left(\frac{Q_y^{(0)}}{h}\right) + \frac{Q_y^{(0)}}{h}\frac{\partial Q_y^{(1)}}{\partial y} = -\frac{2f}{h^2}Q_y^{(1)}\,|\,Q_y^{(0)}\,| \tag{18}$$

The continuity Eq. (14) and the simplified momentum Eq. (18) have two unknowns $Q_x^{(1)}$ and $Q_y^{(1)}$. These equations are subject to the boundary conditions

$$Q_x^{(1)}\,|_{x=0} = 0; \quad Q_y^{(1)}\,|_{y=0} = Q_{yb}^{(1)}(x) \tag{19}$$

in which $Q_{yb}^{(1)}(x)$ is the error in the flux specified at the cross-shore boundaries.

Upon applying $\partial/\partial x$ on Eq. (18) and invoking the continuity Eq. (14) to eliminate $\partial Q_x^{(1)}/\partial x$, we obtain

$$a\frac{\partial^2 Q_y^{(1)}}{\partial x\partial y}+a\frac{2f}{h}\frac{\partial Q_y^{(1)}}{\partial x}-b\frac{\partial Q_y^{(1)}}{\partial y}+\frac{2f}{h}(ch-b)Q_y^{(1)}=0 \tag{20}$$

where $a=V^{(0)}(\partial V^{(0)}/\partial x), b=V^{(0)}(\partial^2 V^{(0)}/\partial x^2), c=(\partial V^{(0)}/\partial x)(\partial/\partial x)(V^{(0)}/h)$, and $V^{(0)}=(Q_y^{(0)}/h)$. Eq. (20) with the boundary condition (19) can be solved by using the method of separation of variables. The solution may be expressed as

$$Q_y^{(1)}=Q_{yb}^{(1)}\mathrm{e}^{-\frac{2f}{h}(1+p)y} \tag{21}$$

in which

$$p=chQ_{yb}^{(1)}\left(a\frac{\partial Q_{yb}^{(1)}}{\partial x}-bQ_{yb}^{(1)}\right)^{-1} \tag{22}$$

For simplicity, assuming $Q_{yb}^{(1)}=\beta Q_y^{(0)}$, where $\beta\ll 1$, leads to

$$p=\frac{h\left(\frac{\partial V^{(0)}}{\partial x}\right)^2-V^{(0)}\frac{\partial h}{\partial x}\frac{\partial V^{(0)}}{\partial x}}{h\left(\frac{\partial V^{(0)}}{\partial x}\right)^2+V^{(0)}\frac{\partial h}{\partial x}\frac{\partial V^{(0)}}{\partial x}-V^{(0)}h\frac{\partial^2 V^{(0)}}{\partial x^2}} \tag{23}$$

Obviously, p depends on the cross-shore distribution of the longshore current. The cross-shore variation of p can be estimated using the theoretical longshore current profile derived by Longuet-Higgins (1970a,b). Rewriting Eq. (23) in term of the dimensionless variables, $\vee=V^{(0)}/V_0$ and $X=x/x_b$, where V_0 is the longshore current velocity at the breaking point resulting from the balance of the cross-shore gradient of radiation stress and the bottom friction, and x_b is the distance between the breaking point and the shoreline, yields

$$p=\frac{X\left(\frac{\partial\vee}{\partial X}\right)^2-\vee\frac{\partial\vee}{\partial X}}{X\left(\frac{\partial\vee}{\partial X}\right)^2+\vee\frac{\partial\vee}{\partial X}-\vee X\frac{\partial^2\vee}{\partial X^2}} \tag{24}$$

Direct use of Longuet-Higgins' (1970a,b) analytical solution of longshore currents allows for the evaluation of Eq. (24). Fig. 1 shows the cross-shore distributions of the normalized velocity corresponding to three different values of the parameter P that is the ratio of the eddy viscosity to the bottom friction on a given planar beach, and the resulting cross-shore variations of p defined by Eq. (24). It is seen that for a realistic value of $P=0.1$, p is close to zero in the area shoreward of the maximum velocity, and increases to its maximum at the breaking point. In the area seaward of the breaking point, however, Longuet-Higgins' solution leads to large negative values of p.

At the location of the maximum velocity, $p=0$, as $\partial V^{(0)}/\partial x=0$. Thus at that location Eq. (21) becomes

$$Q_y^{(1)}=Q_{yb}^{(1)}\mathrm{e}^{-\frac{2f}{h}y} \tag{25}$$

Eq. (25) provides us with a tool to quickly estimate the influence of the error in the upstream boundary conditions on the flow downstream of the boundary without knowing the cross-shore distribution of the longshore current. The simple analytical solution states that errors in the upstream boundary condition decay at an exponential rate in the longshore direction. The stronger the bed shear stress is, the faster the

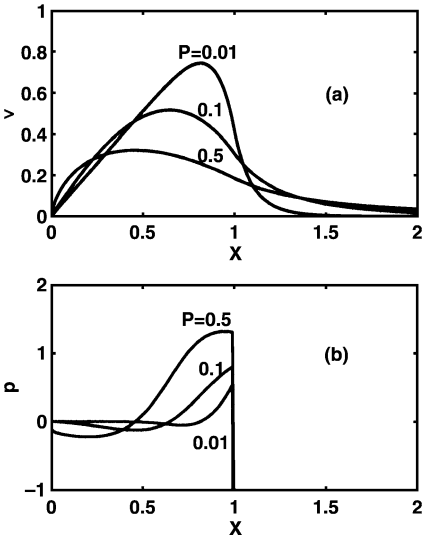

Fig. 1. Longuet-Higgins's solution of longshore currents on a planar beach (a), and the corresponding cross-shore variations of p (b).

boundary influence decays. Also, as $|p| \ll 1$ near the shoreline, the effect of the error in the upstream boundary condition decays faster in the area closer to the shoreline where the water depth is small. It is worth mentioning that the analytical solution (21) or (25) is valid only if the assumptions used to simplify the governing equations are justified. In the following section, we shall verify the analytical model using numerical experiments.

4. Comparisons of analytical and numerical results

4.1. The total flow

The model employed for the numerical experiments is the quasi-3D model SHORECIRC that includes the lateral mixing owing to the depth variations of the currents. The detailed description of the model is given in e.g. van Dongeren and Svendsen (2000).

Visser (1991) was the first to present comprehensive data sets of uniform longshore currents measured in the laboratory. We choose one of his data sets as a reference of our numerical experiments. Fig. 2 shows the computed velocity field and the model/data comparison in the case of Test 4 of Visser's experiments. The numerical wave basin used here is 70 m a longshore and 14 m onshore. The slope of the longshore uniform plane beach is 1/20 and the offshore water depth is 35 cm. The obliquely incident wave train has a wave period of 1.02 s and a wave height of 7.8 cm, and the angle of incidence is 15.4°. Because of the high degree of longshore uniformity of the current measured by Visser, longshore periodicity is assumed along the cross-shore boundaries.

The numerical model SHORECIRC is then driven by the gradients of the radiation stresses that are the output of the short wave model REFDIF. Wave breaking occurs about 2 m seaward of the shoreline and the obliquely incident wave generates a uniform longshore current. Sufficiently long computation is carried out to ensure that the current reaches its steady state. No shear instabilities occur in the model. As shown by the bottom panels in Fig. 2, the computed wave height, wave setup, and cross-shore distribution of the velocity agree well with Visser's measurements except for a slight over-prediction of the longshore current in the offshore region. The corresponding bottom friction coefficient in Eqs. (6) and (7) is 0.00325 (i.e. $f_w = 0.0065$ in SHORECIRC).

The numerical solution with the periodic cross-shore boundary condition as shown in the top panel of Fig. 2 is defined as the undisturbed flow field which

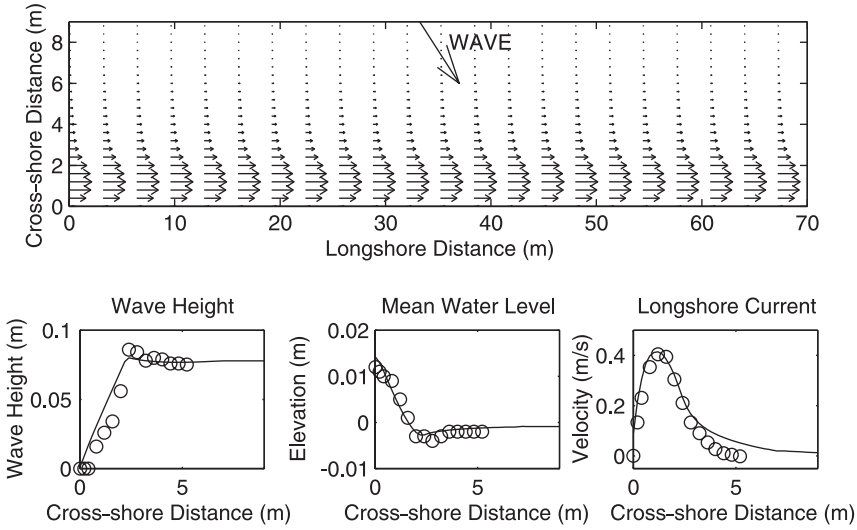

Fig. 2. Top panel: Computed velocity field of uniform longshore current. Bottom panels: Comparison of Visser's (1991) laboratory measurements (○) and the numerical solutions (—) with periodic cross-shore boundaries.

shall be used as the true solution, or the reference in the numerical experiments with boundary errors. By replacing the longshore periodicity along the shore-normal boundaries with a specified flux boundary condition, we can intentionally either increase or decrease the flux at both upstream and downstream boundaries. In the following numerical examples, we have changed both upstream and downstream boundary conditions by 10% from the true solution. The input wave condition and all model parameters remain unchanged. We shall refer to the case with the increased flux at the shore-normal boundaries as excessive flux and to the case with the decreased flux boundary condition as reduced flux.

Fig. 3 illustrates the total velocity field and the cross-shore distribution of the computed velocity at three different longshore locations in the case of excessive flux. As a reference, the cross-shore distribution for the undisturbed flow is also shown for three cross sections in the bottom panels (dashed line) along with the cross-shore distribution of the perturbed flow (full line). Because the perturbation at the upstream and downstream boundaries is small, the signature of the boundary mismatch is not (or hardly) noticeable in the total flow field shown in the top panel of Fig. 3. The velocity profiles, however, clearly depict the deviation of the velocity from the true solution at both the upstream and downstream boundaries. It is interesting that this deviation vanishes in the middle of the wave basin where the cross-shore transect is far away from the upstream and downstream boundaries. The numerical model also gives similar results in the case of reduced flux, which is not shown here.

Notice that although an identical flux condition is specified at both the upstream and downstream boundaries, the velocity profiles appear to be somewhat different as shown by the solid lines in the left and right bottom panels in Fig. 3. This is attributed to a decrease in the water depth caused by the significant decrease of the mean water level at the downstream boundary. This is further discussed below.

4.2. The spreading of boundary errors

To analyze the spatial distribution of the error caused by the imposed boundary mismatch, we subtract the true solution of the undisturbed flow from the solutions with the boundary errors. Fig. 4 shows the resultant residual velocity field in the case of excessive flux. A similar residual velocity field that is not shown here is also obtained in the case of reduced flux. The upper panels of Fig. 4 illustrate the spatial

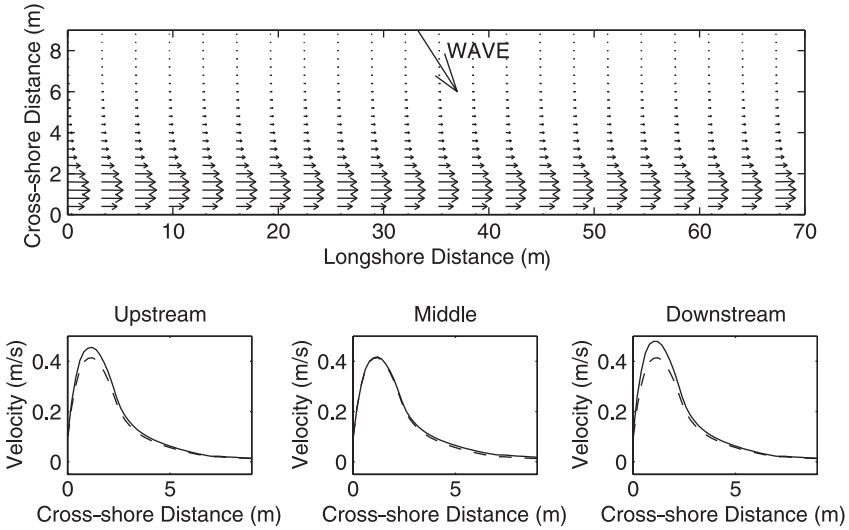

Fig. 3. Top panel: Computed total velocity field of longshore current with excessive flux at the cross-shore boundaries. Bottom panels: Comparison of the cross-shore distributions of the longshore velocity at three locations in the case of periodic cross-shore boundaries (- - -) and excessive flux boundaries (—).

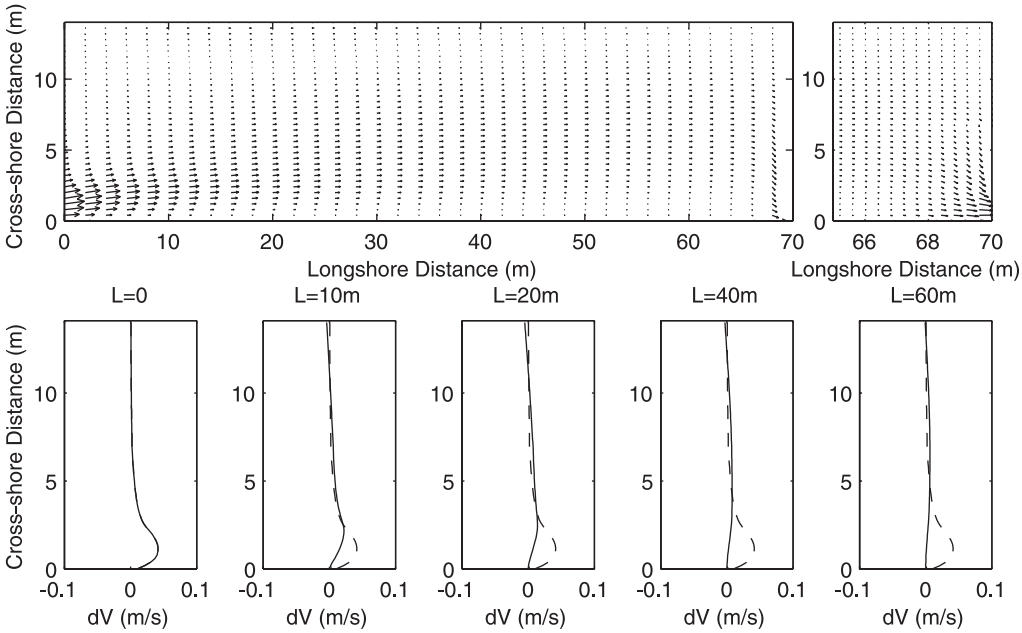

Fig. 4. Top panels: Computed residual velocity field in the case of excessive flux. Bottom panels: Cross-shore distributions of the residual velocity at five longshore locations. (- - -): The residual velocity at the upstream boundary.

distribution of the residual flow, or the errors caused by the disturbance at the shore-normal boundaries, and the bottom panels depict the cross-shore profiles of the longshore component of the residual velocity at six different longshore locations.

We notice that the error introduced at the upstream boundary originally is concentrated near the shoreline in the area close to the upstream boundary because the assumed disturbance is 10% of the undisturbed velocity. Into the computational domain the upstream boundary error spreads in the manner that it tends to disperse the error away from the surf zone. This is illustrated more clearly by the residual velocity profiles in the bottom panels of Fig. 4, where the dashed lines are the residual velocity profile at the upstream boundary as a reference. For instance, at the location of 40 m away from the upstream boundary, the residual velocity in the surf zone becomes nearly zero.

In contrast to the influence of the upstream boundary error, close to the downstream boundary the error is apparently confined to a small area upstream of the downstream boundary. We have to blow up the area adjacent to the downstream boundary in order to examine the residual velocity field in that area as shown in the right top panel of Fig. 4. We see that the area disturbed by the downstream boundary error is much smaller than that influenced by the upstream boundary error. In popular terms in this region the residual flow has similarities with the flow out of a bathtub because the major part of the residual outflow occurs around the relatively narrow region of maximum velocity in the undisturbed flow.

The distinction between the influences of the upstream and downstream boundary mismatch is interesting because it contradicts the boundary effects of a hyperbolic system for a subcritical flow. The influences of both the upstream and downstream boundaries in a subcritical flow of a hyperbolic system, such as long wave motions, can propagate through the entire computational domain. The model result suggests that the longshore current system behaves more like a parabolic system in which the upstream boundary has a dominant effect over the downstream boundary. The implication of the difference in the effects of upstream and downstream boundaries on longshore current simulations is that to prevent the flow in a computational domain from

being contaminated by the unavoidable boundary errors, the upstream boundary has to be placed much further away from the area of interest than the downstream boundary.

The residual velocity field for the case of reduced flux is shown in Fig. 5. It shows that for so small residuals as 10% the excess and reduced flow cases show almost identical patterns with an opposite sign. At the cross-shore boundaries, the requirement of mass conservation dictates a return flow near the offshore boundary.

Our discussion so far has focused on the spatial structure of the residual velocity in the area near the shoreline (i.e. 1–2 times the surf zone width). If we take a close look at the residual flow in the offshore area in Fig. 4, it is found that while the residual velocity flux seem to vanish in the area far away from the cross-shore boundaries, the residual volume flux does not vanish because volume flux is conserved. This is illustrated in Fig. 6, which shows the distribution of the excess volume fluxes in the computational domain. This figure also illustrates that the volume fluxes corresponding to the small velocities in the offshore regions are actually quite substantial because of the monotonously increasing depth. Hence for the volume flux it is obvious that the flux is just dispersed to conserve mass and nothing is lost at any cross section.

The upper panels in Fig. 7 show the comparison of the analytical and numerical residual fluxes normalized by the boundary mismatch dQ_b. Three longshore transects at different cross-shore locations $x/x_p = 0.5$, 1.0 and 1.5 are presented, where x is the distance from the shoreline and x_p is the location of the peak velocity. The dashed lines are the numerical results and the solid lines are the analytical solutions of Eq. (25) (thick lines) and Eq. (21) (thin lines). Both cases of excessive and reduced fluxes give an identical set of dashed lines for these three transects.

It is seen that both the analytical solutions given by Eqs. (21) and (25) agree very well with the numerical results in the area shoreward of the peak velocity except for the region adjacent to the downstream boundary where the analytical model is invalid. In the area seaward of x_p, surprisingly, the simplified solution given by Eq. (25) is in better agreement with

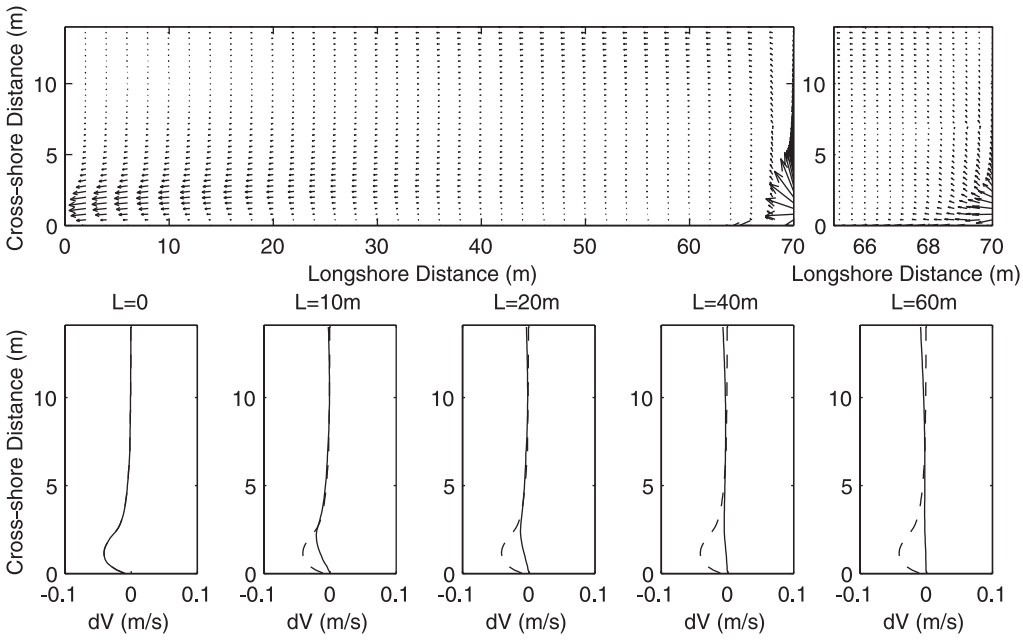

Fig. 5. Top panels: Computed residual velocity field in the case of reduced flux. Bottom panels: Cross-shore distributions of the residual velocity at five longshore locations. (- - -): The residual velocity profile at the upstream boundary.

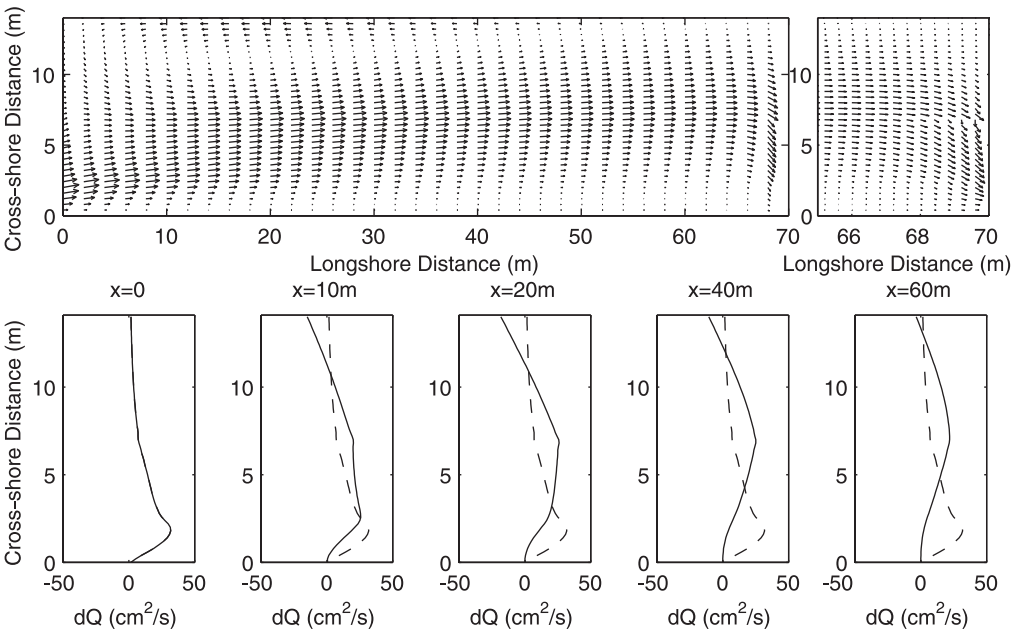

Fig. 6. Top panels: Computed residual flux field in the case of excess flux. Bottom panels: Cross-shore distributions of the residual velocity at five longshore locations. (—): The residual velocity profile at the upstream boundary.

the numerical model than is the full solution that takes the cross-shore variation of the uniform longshore current into account. A close inspection on the contribution by the cross-shore variation of the longshore current indicates that there are considerable irregularities in the numerical results for the area seaward of x_p. This may be attributed to small numerical oscillations imbedded in the velocity profile that are amplified by the term containing the first and second derivatives of the velocity with respect to x. Nevertheless, the simplified result (Eq. (21)) is more useful than the full solution (Eq. (25)) because the longshore

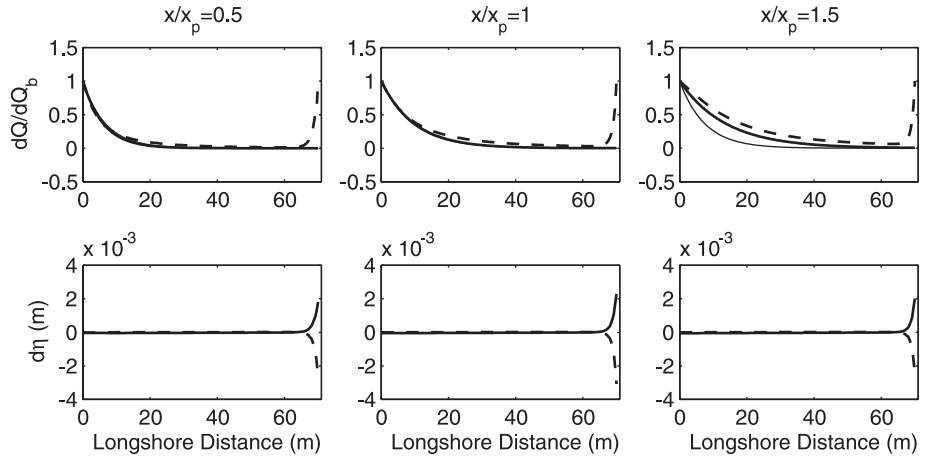

Fig. 7. Top panels: Comparison of the residual fluxes given by the analytical and numerical models. Thick solid lines: Eq. (25); thin solid lines: Eq. (21); dashed lines: numerical result. Bottom panels: The changes in the mean water level in the cases of excessive (- - -) and reduced (—) fluxes.

current is simply unknown before the numerical simulation.

The bottom panels in Fig. 7 show the comparison of the residual mean water levels corresponding to the excessive (dashed lines) and reduced (solid lines) fluxes along the three longshore transects. It is seen that the mean water level is not affected by the upstream boundary mismatch. However, the excessive flux results in a considerable drawdown of the mean water surface near the downstream boundary while the reduced flux leads to an elevated mean water level in that area. Obviously, the downstream boundary mismatch causes rapid changes in the mean water level within a short distance, which leads to a large longshore pressure gradient in the area adjacent to the downstream boundary.

In the offshore area, the analytical model deviates from the numerical solution, which is not shown. The reason will be given by the analysis of the balance of the residual momentum flux in the following subsection.

4.3. The variations of the residual momentum flux

The first-order momentum equations resulting from the perturbation analysis in the preceding section governs the spreading of boundary errors. To obtain insight into the residual flow, we analyze the balance of the residual momentum flux on the basis of the numerical results given by SHORECIRC. By subtracting the true solution, or the longshore uniform flow from the flow with the boundary mismatch, we obtain the residual flux, residual velocity, and residual mean water level. The residual flow field is then used to evaluate each term in the first-order momentum equations.

Fig. 8 illustrates the cross-shore variations of each term in the longshore component of the first-order momentum Eq. (16) at six different longshore locations. The thick dashed lines represent the convective terms. The longshore pressure gradient is shown by the dotted lines and the bottom friction is shown by the thick solid lines. The thin solid lines depict the residual diffusion. First, we notice that the convective terms play an import role in the residual flow. Second, it is seen that the longshore pressure gradient is rather weak except in the area adjacent to the downstream boundary (e.g. $L=68$ m) where the bottom friction becomes unimportant in comparison with other terms. Third, the residual momentum flux becomes virtually zero in the area far away from the upstream boundary (e.g. $L=60$ m) although the location is quite close to the downstream boundary.

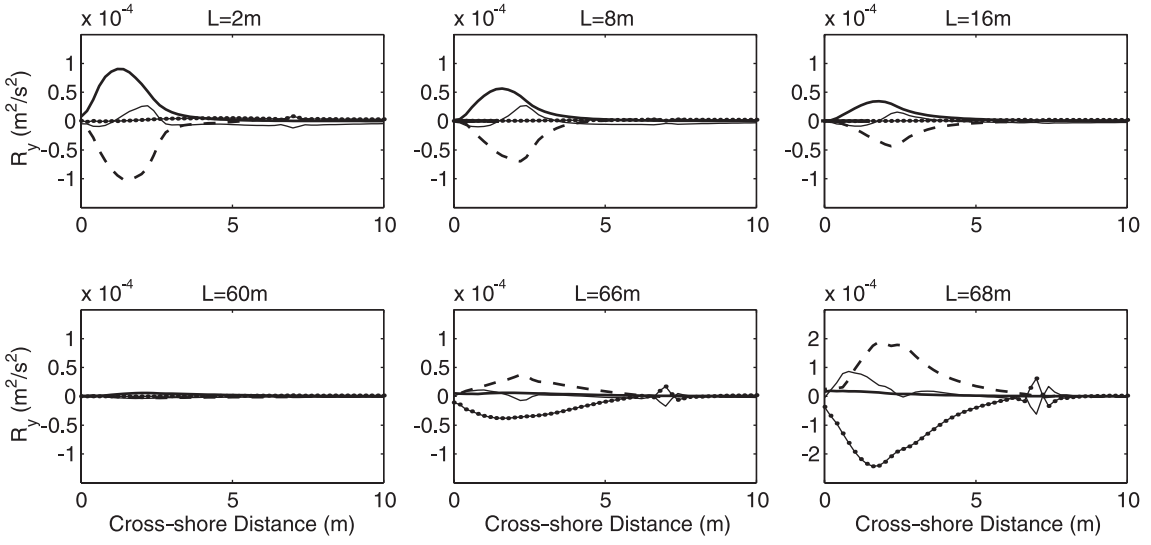

Fig. 8. Computed cross-shore variations of the terms (R_y) in Eq. (16) in the case of excessive flux. Thick dashed lines: $Q_x^{(1)}(\partial/\partial x)(Q_y^{(0)}/h)+(Q_y^{(0)}/h)(\partial Q_y^{(1)}/\partial y)$; dotted lines: $gh\,(\partial\zeta^{(1)}/\partial y)$; thick solid lines: $(2f/h^2)Q_y^{(1)}|Q_y^{(0)}|$; thin solid lines: $M_y^{(1)}$.

On the basis of the computed first-order momentum flux, the residual flow field may be divided into three different regimes. The first one is the longshore strip near the shoreline, covering 1–2 times the surf zone width. In this area starting from the upstream boundary, the longshore pressure gradient is negligible in comparison to other terms in the momentum equation. Thus the residual flow results from a balance of the convective terms, the bottom friction, and the diffusion term. We notice that the diffusion is also relatively weak in comparison to the convection and bottom friction in this area. This supports the assumption of the analytical model. In other words, the analytical model is applicable in this regime where both the residual convection and bottom friction are dominant.

The second distinct regime of the residual flow is the area adjacent to the downstream boundary. The numerical results show that the longshore pressure gradient balances the convective term in this area where the bottom friction and diffusion are negligible. Thus the first-order momentum Eqs. (15) and (16) may be simplified as follows.

$$\frac{Q_y^{(0)}}{h}\frac{\partial Q_x^{(1)}}{\partial y}+gh\frac{\partial \zeta^{(1)}}{\partial x}=0 \tag{26}$$

$$Q_x^{(1)}\frac{\partial}{\partial x}\left(\frac{Q_y^{(0)}}{h}\right)+\frac{Q_y^{(0)}}{h}\frac{\partial Q_y^{(1)}}{\partial y}+gh\frac{\partial \zeta^{(1)}}{\partial y}=0 \tag{27}$$

Using Eq. (14) to eliminate $Q_y^{(1)}$ in Eq. (27), and cross-differentiating the resulting equation and Eq. (26) to eliminate $\eta^{(1)}$ lead to a second-order PDE

$$\frac{\partial^2 Q_x^{(1)}}{\partial x^2}+\frac{\partial^2 Q_x^{(1)}}{\partial y^2}-A\frac{\partial Q_x^{(1)}}{\partial x}-BQ_x^{(1)}=0 \tag{28}$$

where $A=(1/h)(\partial h/\partial x)$ and $B=(h^2/Q_y^{(0)})(\partial/\partial x)[(1/h)(\partial/\partial x)(Q_y^{(0)}/h)]$.

Eq. (28) is subject to the following boundary conditions: $Q_x^{(1)}=0$ at both the shoreline and offshore boundaries, $Q_x^{(1)}=Q_{xb}^{(1)}$ at the downstream boundary ($y=L$), and $Q_x^{(1)}=0$ at $y=L-\delta$, where δ is a short distance from the downstream boundary. The method of separation of variables in combination with a numerical method for the determination of the eigenvalues can be used to solve the second-order PDE governing the residual flow in the second regime, but it is omitted here.

The rest of the area in the offshore region of the computational domain may be considered as a third regime of the residual flow. In this area, no term in the first-order momentum equations can be neglected because all of them are of the same order of magnitude. Thus no simple analytical solution can be obtained for this flow regime. A close inspection of the numerical results indicates that there exists a circulation in this complex flow regime where the convection and momentum mixing play an important role.

4.4. The entrainment and balance of volume flux

If we consider the total residual flux, calculated as the integral of the volume flux from the shoreline out to a certain distance, it is found that this flux actually increases as we move downstream. The reason for this is that the way the excess flow is specified allows the excess flux to act as a relatively narrow jet centered around the region of maximum longshore current velocity, which entrains additional flux from the seaward region. Hence the further downstream, the larger the total excess volume flux will seem to be. To compensate for this, a return flow is generated in the farthest offshore region of the computational domain. To conserve volume flux, all the entrained flux is again transferred to the return flow before the flow reaches the downstream boundary, because only the excess volume flux initially infused at the upstream boundary is also taken out at the downstream boundary. This is essentially in agreement with the laboratory experiments by Visser (1991), who developed a technique to minimize the return flow by adjusting the cross-shore distribution of his in- and outflow conditions in the basin and to determine the optimal conditions for longshore uniform flow. A similar approach was used by Reniers and Battjes (1997) and Hamilton and Ebersole (2001).

However, because this process is also associated with an increase in the width of the excess jet, there is a limit to how far downstream this process can continue without being constrained by the cross-shore width of the computational domain. Further numerical experiments with different cross-shore width of the computational domain reveal the dependence of the

strength of the circulation on the width of the domain. It is found that the entrained volume flux increases with the cross-shore domain width L_x relative to the domain length L_y.

The upper panel in Fig. 9 depicts the longshore variations of the volume rates of the forward and backward residual flow with different cross-shore width of the domain. We define the integral of all the positive residual flux at each cross-shore section as the forward flux and the integral of all the negative residual flux as the backward or return flux. The solid lines represent the forward and backward fluxes in the case of $L_x/L_y = 0.44$, where L_x is the cross-shore width of the domain and L_y is the longshore length of the domain. Similarly, the dashed and dotted lines respectively show the cases of $L_x/L_y = 0.3$ and 0.2. Both the forward and backward fluxes increase with the distance from the cross-shore boundaries and reach their maximum near the midway of the basin.

The bottom panels in Fig. 9 show the ratio of the forward and backward fluxes to the disturbance at the cross-shore boundaries as a function of the cross-shore width normalized by the longshore length of the domain. Obviously, both the forward and backward fluxes increase with the width of the computational domain. For instance, with $L_x/L_y = 0.3$, the maximum volume rate of the forward residual flow is about 1.4 times the total volume rate of the error specified at the cross-shore boundaries. The rate of the increase of the forward and backward flux with the basin width seems to slow down when a larger basin width is used. A secondary circulation cell may develop with a large ratio of L_x/L_y, as demonstrated by Hamilton and Ebersole's (2001) laboratory experiment.

5. Conclusions

The paper analyzes how an unavoidable error in the cross-shore boundary condition influences the accuracy of the predicted flow conditions inside the computational domain. The analyses focus on the simple case of a longshore uniform beach. We began with a perturbation analysis of the simplified equations for nearshore circulation to determine the equations governing the spatial distribution of the boundary error. An analytical solution for the flow downstream of the inflow boundary was derived. A simple approximation was also developed to have a quick estimate of the influence distance from the upstream boundary. The analytical results were com-

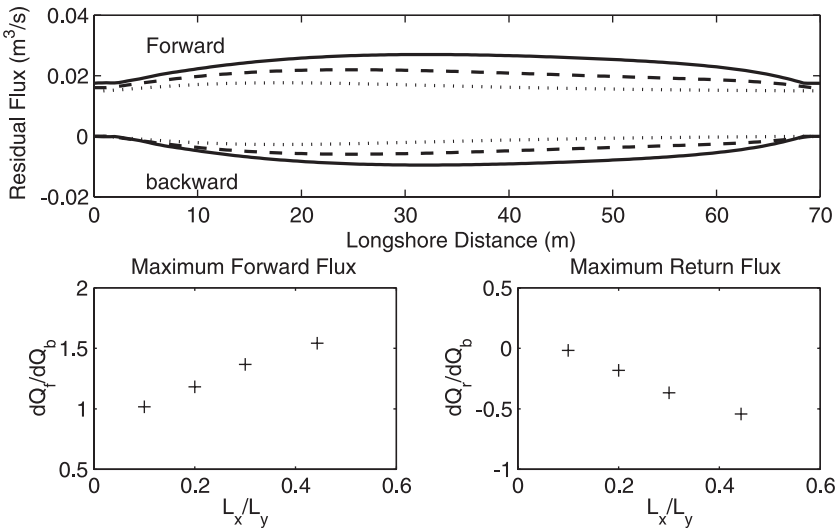

Fig. 9. Top panel: Longshore variations of the forward and backward fluxes with different cross-shore width of the domain. Solid lines: $L_x/L_y = 0.44$; dashed lines: 0.3; dotted lines: 0.2. Bottom panels: The maximum magnitudes of the forward flux (left) and backward flux (right) versus the cross-shore width of the domain.

pared with a series of numerical experiments on the effects of the cross-shore boundaries on the flow field using a nearshore circulation model SHORECIRC. With an error distribution specified at each cross-shore point of the boundary as a small fraction (10%) of the longshore velocity, the numerical results suggest that the boundary error at the upstream cross-shore boundary tends to propagate away from the surf zone and the influence of the error at the downstream cross-shore boundary is limited to the area adjacent to the downstream boundary.

Both the analytical and numerical solutions show that errors in the longshore current specified at the upstream boundary decay exponentially in the surf zone where the bottom friction and convective terms are dominating in the residual momentum equation. In contrast, the longshore pressure gradient balances the convection in the area adjacent to the downstream boundary where boundary mismatches cause considerable changes in the mean water level. A rule-of-thumb can be developed to estimate the effect of upstream boundary errors based on Eq. (25). For a bed shear stress coefficient $f = 0.003$ and a beach slope of 1/50, the longshore distance from the upstream boundary should exceed 10 times the surfzone width to avoid the contamination of the boundary errors in the maximum longshore current. A reduction of the bottom friction coefficient will result in an increase of the needed longshore distance.

Numerical experiments suggest that, in the case of excessive flux given at the cross-shore boundaries, a circulation cell tends to develop in the offshore region where the errors generated by the boundary mismatch increase with the cross-shore width of the model domain. The results have similar characteristics as found in laboratory experiments with longshore currents. The analyses of the momentum balance and the mass balance on the basis of the numerical solutions not only confirm the hypothesis used to obtain the analytical model, but also provide insight into the complex residual flow field generated by errors in the cross-shore boundary conditions.

Acknowledgements

Funding for this study was provided by the Office of Naval Research through grant N00014-99-1-0398. Discussions with Drs. Fengyan Shi and Kevin Haas are acknowledged.

References

Dalrymple, R.A., Eubanks, R.A., Birkemeier, W.A., 1977. Wave-induced circulation in shallow basins. J. Waterw., Port, Coast., Ocean Div. 103, 117–135 (ASCE).

Hamilton, D.G., Ebersole, B.A., 2001. Establishing uniform longshore currents in a large-scale sediment transport facility. Coast. Eng. 42, 199–218.

Kirby, J.T., Dalrymple, R.A., 1994. Combined refraction/diffraction model ref/dif 1, version 2.5, Technical Report CACR-94-22, Center for Applied Coastal Research, University of Delaware.

Longuet-Higgins, M.S., 1970a. Longshore currents generated by obliquely incident sea waves, 1. J. Geophys. Res. 75, 6778–6789.

Longuet-Higgins, M.S., 1970b. Longshore currents generated by obliquely incident sea waves, 2. J. Geophys. Res. 75, 6790–6801.

Reniers, A.J.H.M., Battjes, J.A., 1997. A laboratory study of longshore currents over barred and non-barred beaches. Coast. Eng. 30, 1–22.

Svendsen, I.A., Putrevu, U., 1994. Nearshore mixing and dispersion. Proc. R. Soc. Lond., A 445, 1–16.

van Dongeren, A.R., Svendsen, I.A., 2000. Nonlinear and quasi 3D effects in leaky infragravity waves. Coast. Eng. 41, 467–496.

Visser, P.J., 1991. Laboratory measurements of uniform longshore currents. Coast. Eng. 15, 563–593.